

# UP-CrackNet: Unsupervised Pixel-Wise Road Crack Detection via Adversarial Image Restoration

Nachuan Ma, *Graduate Student Member, IEEE*, Rui Fan, *Senior Member, IEEE*, and Lihua Xie, *Fellow, IEEE*

**Abstract**—Over the past decade, automated methods have been developed to detect cracks more efficiently, accurately, and objectively, with the ultimate goal of replacing conventional manual visual inspection techniques. Among these methods, semantic segmentation algorithms have demonstrated promising results in pixel-wise crack detection tasks. However, training such networks requires a large amount of human-annotated datasets with pixel-level annotations, which is a highly labor-intensive and time-consuming process. Moreover, supervised learning-based methods often struggle with poor generalizability in unseen datasets. Therefore, we propose an unsupervised pixel-wise road crack detection network, known as UP-CrackNet. Our approach first generates multi-scale square masks and randomly selects them to corrupt undamaged road images by removing certain regions. Subsequently, a generative adversarial network is trained to restore the corrupted regions by leveraging the semantic context learned from surrounding uncorrupted regions. During the testing phase, an error map is generated by calculating the difference between the input and restored images, which allows for pixel-wise crack detection. Our comprehensive experimental results demonstrate that UP-CrackNet outperforms other general-purpose unsupervised anomaly detection algorithms, and exhibits satisfactory performance and superior generalizability when compared with state-of-the-art supervised crack segmentation algorithms. Our source code is publicly available at [mias.group/UP-CrackNet](https://github.com/mias.group/UP-CrackNet).

**Index Terms**—semantic segmentation, crack detection, generative adversarial network, and unsupervised anomaly detection.

## I. INTRODUCTION

CRACKS are slender, dark lines or curves that appear on the surface of solid materials, such as roads and bridges [1]. Road cracks result from the interplay of water and traffic influences [2], including soil swelling, foundation shifting, traffic overcrowding, premature drying, material expansion and contraction, *etc.* Road cracks are not just an inconvenience, they significantly affect the reliability and sustainability of civil infrastructure while posing a significant threat to vehicle conditions and driving safety [3]. For instance, in the first

two months of 2018, drivers in Chicago submitted 11,706 complaints pertaining to road defects. Furthermore, statistics suggest that substandard road conditions are responsible for nearly one-third of the 33,000 traffic fatalities that occur in the United States annually [4], [5]. Therefore, to lower the risk of structural degradation and traffic accidents, frequent road inspection is necessary and essential [6]. Currently, manual visual inspection is still the dominant method for road crack detection [7]. The locations of road cracks are recorded routinely by civil engineers or qualified inspectors, the process of which is time-consuming, costly, and hazardous [8], [9]. For example, New Zealand city councils spent millions of dollars in 2017 detecting and repairing road defects (Christchurch alone spent 525,000 USD) [5]. Moreover, the detection results are always qualitative and subjective, as decisions depend entirely on personal opinions and expertise. Owing to these concerns, there is an ever-increasing need to develop automated road condition monitoring methods that can detect road cracks accurately, efficiently, and objectively [10].

Before the advent of the deep learning revolution, research in road crack detection was primarily dominated by traditional image processing-based techniques, including edge-based [11], [12], thresholding-based [13], texture analysis-based [14], wavelet-based [15], and minimal path search-based methods [16]. While these methods may demonstrate effectiveness in certain simple scenarios, they are often characterized by high computational demands and susceptibility to various environmental factors, with illumination and weather conditions being particularly notable [17]. Moreover, the geometric presumptions used in such methods are sometimes impractical, due to the irregular shapes of road cracks [18].

Fortunately, with recent advances in deep learning, convolutional neural networks (CNNs) have been extensively employed as feasible methods for automated road crack detection. Rather than setting explicit parameters and using hand-crafted features, CNNs are typically trained to update the implicit parameters of neural layers through back-propagation with a huge amount of human-annotated road data. Such data-driven algorithms are commonly divided into three categories: (1) image classification networks, (2) object detection networks, and (3) semantic segmentation networks. The image classification networks [19] are trained to distinguish positive (crack) and negative (non-crack) road images [20]. Object detection networks are trained to identify road cracks at the instance level (location and class) [21], [22]. Semantic segmentation networks [23]–[29] are trained to achieve pixel-wise crack detection results, and they have emerged as the preferred choice for this task in recent years.

Nonetheless, the aforementioned pixel-wise road crack de-

arXiv:2401.15647v2 [cs.CV] 6 May 2024

Manuscript received June 26, 2023; revised November 04, 2023, January 09, 2024, and April 18, 2024; accepted April 28, 2024. This research was supported by the Fundamental Research Funds for the Central Universities and Xiaomi Young Talents Program. (*Corresponding author: Rui Fan*)

N. Ma and R. Fan are with the College of Electronics & Information Engineering, Shanghai Research Institute for Intelligent Autonomous Systems, the State Key Laboratory of Intelligent Autonomous Systems, and Frontiers Science Center for Intelligent Autonomous Systems, Tongji University, Shanghai 201804, China. (e-mails: [manachuan@163.com](mailto:manachuan@163.com), [ruifan@ieee.org](mailto:ruifan@ieee.org))

L. Xie is with the School of Electrical and Electronic Engineering, Nanyang Technological University, 50 Nanyang Avenue, Singapore 639798 (e-mail: [elhxie@ntu.edu.sg](mailto:elhxie@ntu.edu.sg)).

Color versions of one or more figures in this article are available at <https://doi.org/10.1109/TITS.2024.3398037>.

Digital Object Identifier 10.1109/TITS.2024.3398037

tection algorithms predominantly rely on supervised learning. On one hand, training these data-driven algorithms demands a large amount of pixel-level human-annotated labels. The annotation process is exceptionally labor-intensive and time-consuming. Moreover, unique road cracks are not ubiquitous, which adds complexity to the task of gathering a sufficient number of images containing road cracks. On the other hand, supervised learning-based algorithms often demonstrate limited generalizability when applied to different scenarios due to their dependency on fixed, pre-defined patterns learned from specific training data, which may not adequately represent the variability and complexity of real-world situations.

To overcome these limitations, we propose an **Unsupervised Pixel-wise Crack Detection Network (UP-CrackNet)** via adversarial image restoration. In the training phase, multi-scale square masks are first generated and selected randomly to corrupt input undamaged road images. These corrupted images are subsequently fed into the proposed model, which learns semantic context from surrounding uncorrupted regions to restore the corrupted regions while adhering to a global consistency constraint. In the testing phase, when provided with a damaged road image, the trained model can restore undamaged regions but may not effectively restore crack regions to their original appearance. Consequently, we can obtain an error map by comparing the difference between the input damaged image and the restored image. This error map can then be used to produce pixel-wise crack detection results. We conduct experiments on three public road crack detection datasets. The results suggest that UP-CrackNet can eliminate the need for human annotations during training while outperforming other unsupervised anomaly detection algorithms. Furthermore, it achieves satisfactory performance and shows superior generalizability when compared to state-of-the-art (SoTA) supervised crack detection approaches. Our main contributions are summarized as follows:

- 1) We propose UP-CrackNet, a novel unsupervised network for pixel-wise road crack detection via adversarial image restoration. It uses only undamaged road images in the training phase without any human-annotated labels.
- 2) We design multi-scale square masks to randomly corrupt input undamaged images, which can prevent the network from degenerating into an identity mapping in the inference phase.
- 3) We design comprehensive loss functions, enabling the network to learn semantic context features from uncorrupted undamaged regions to restore the corrupted regions.
- 4) We conduct extensive experiments and compare our method with 11 supervised methods and two unsupervised methods. The results suggest that UP-CrackNet outperforms other unsupervised methods and demonstrates satisfactory performance and superior generalizability compared to supervised methods.

The remainder of this article is organized as follows: Sect. II reviews related works. Sect. III provides a detailed description of our proposed network and loss functions. Sect. IV presents implementation details, evaluation metrics, experimental re-

sults, and visualization analysis. Sect. V discusses failure cases and Sect. VI concludes the article.

## II. LITERATURE REVIEW

### A. Traditional Road Crack Detection Methods

Traditional road crack detection methods are generally based on visual features, with edges being a common choice. For instance, bi-dimensional empirical mode decomposition along with the Sobel edge detector was used in [12] to identify road cracks. Thresholding methods are also prevalently employed for this task. Assuming that road cracks consist of thin interconnected textures, in [13], crack textures were extracted by analyzing the connectivity of luminance and shape within the infiltrated regions. Texture analysis-based techniques are another alternative. In [14], local binary pattern operators were utilized to group road patterns and extract distinctive local features for crack detection. Additionally, wavelet-based approaches [15], [30] decompose road images into different frequency sub-bands to enable the identification of road cracks. Minimal path search-based methods [16], [31] are also a popular choice for road crack detection. These methods begin by identifying relatively dark pixels as the endpoints of road cracks and subsequently compute minimal paths between them using path planning techniques to generate road cracks. Nevertheless, the aforementioned traditional road crack detection methods are sensitive to environmental factors and may occasionally prove ineffective, particularly when faced with irregularly shaped road cracks.

### B. Supervised Road Crack Detection Methods

CNNs developed for general computer vision tasks, such as image classification, object detection, and semantic segmentation, have been widely adopted in road crack detection. Image classification networks are employed to categorize road image patches as either negative (indicating healthy road surfaces) or positive (indicating patches containing cracks) [17], [20], while object detection networks further localize road cracks with bounding boxes [22], [32], [33]. Although these networks are unable to produce pixel-wise results, they can be utilized in the preparation of datasets for our proposed unsupervised road crack detection framework.

Semantic segmentation networks, trained through supervised learning, have the capacity to generate pixel-wise road crack detection results. Deepcrack [3] incorporates a side-output layer into the VGG-16 [34] model and utilizes conditional random fields and guided filtering to achieve accurate road crack detection results. Another Deepcrack version, proposed in [1], fuses features from various scales of SegNet [35] to acquire hierarchical information, leading to improved road crack segmentation performance. RHA-Net [36] integrates residual blocks and hybrid attention modules into an encoder-decoder network for pixel-wise road crack detection. Similarly, DMA-Net [37] integrates a multi-scale attention module into the decoder of Deeplabv3+ [38] to dynamically adjust weights across different feature maps for better crack detection results. However, training such methods requires a large amount of human-annotated pixel-level annotations, which is a highly

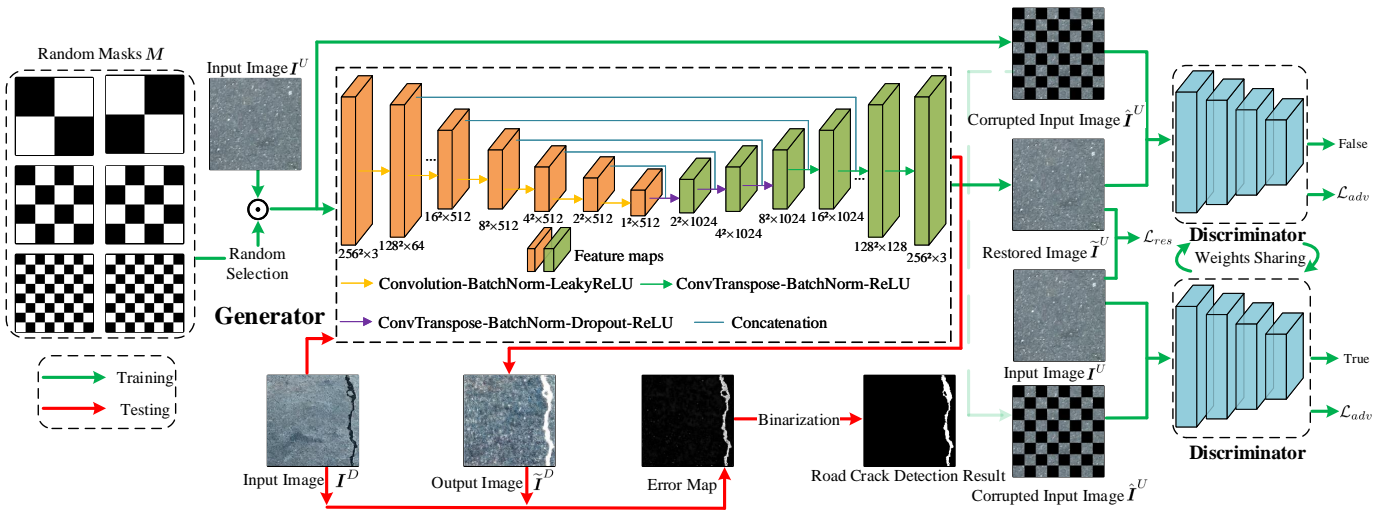


Fig. 1: An illustrative pipeline of our proposed UP-CrackNet.

labor-intensive and time-consuming process. Moreover, they often struggle with poor generalizability in unseen datasets.

### C. Unsupervised Anomaly Detection Methods Based on Image Restoration

Unsupervised anomaly detection approaches based on image restoration have been prevalently used for industrial defect detection. These methods can be categorized into autoencoder (AE)-based [39], [40], variational autoencoder (VAE)-based [41], [42], and generative adversarial network (GAN)-based [43]. Among them, GAN-based approaches generate images with the highest quality. However, these methods often generalize to abnormal samples or even degenerate into an identity mapping during the inference phase. To overcome this limitation, researchers attempted to introduce perturbations [44]–[47], which help maintain the dissimilarity between model inputs and outputs, thereby improving the learning of contextual information from normal samples. In [46], a semantic context-based anomaly detection network (SCADN) based on striped masks was proposed. It removes specific regions from the input images and trains a GAN model to restore the corrupted regions. [47] proposed a reconstruction-by-inpainting anomaly detection (RIAD) method, using jumbled small square masks to randomly remove regions of input images and training an AE model with U-Net architecture to restore the corrupted regions. Drawing inspiration from these approaches, we introduce UP-CrackNet, a novel unsupervised pixel-wise road crack detection approach based on adversarial image restoration. UP-CrackNet is trained on undamaged road images during the training phase, without the reliance on any human-annotated labels.

## III. METHODOLOGY

### A. Architecture Overview

The training and testing processes of our proposed UP-CrackNet are illustrated in Fig. 1. During the training phase, we first create corrupted images by performing the Hadamard

product operation between the input undamaged road images and randomly generated square masks (where mask values are set to either 0 or 1). Subsequently, we train the proposed model to restore the corrupted regions by minimizing a restoration loss and an adversarial loss. In the testing phase, when provided with damaged road images, the model generates restored images using the learned parameters. Error maps are then obtained by computing the differences between the damaged road images and the restored images. Finally, post-processing techniques are applied to these error maps to enhance the crack detection results.

### B. Undamaged Road Image Random Corruption

When designing masks for the random corruption of input undamaged road images, we take into consideration the need for image regions to have an equal chance of being removed. This ensures that all undamaged regions in the training set have an equal probability of being learned by the model. Specifically, an image is divided into  $\frac{H}{k} \times \frac{W}{k}$  patches, where  $H$  and  $W$  represent the height and width of input undamaged road images, respectively, and  $k$  determines the density of patches. We use a boolean logic strategy to design masks, where pixel values are set to 0 or 1 to indicate the regions that should be removed or retained, respectively. The ratio between the removed and retained regions is 1 : 1. Given the undamaged road crack training set  $\mathcal{I}^U$ , the random corruption process can be formulated as  $\hat{\mathbf{I}}^U = \mathbf{I}^U \odot \mathbf{M}$ , where  $\mathbf{I}^U \in \mathcal{I}^U$  denotes the input undamaged road image,  $\mathbf{M}$  denotes the selected mask,  $\odot$  denotes the Hadamard product, and  $\hat{\mathbf{I}}^U$  denotes the corrupted input undamaged image.

### C. Adversarial Image Restoration

Our proposed UP-CrackNet consists of a generator  $G$  and a discriminator  $D$ .  $G$  is trained to restore the corrupted regions by minimizing a restoration loss and an adversarial loss, while  $D$  is designed to discriminate between input undamaged road

images and the restored images generated by  $G$ , with the aim of maximizing the adversarial loss.

Generator  $G$  consists of an encoder and a decoder. The encoder uses modules of the form Convolution-BatchNorm-LeakyReLU, where the BatchNorm layer performs normalization for each mini-batch to expedite training, and the LeakyReLU layer prevents the vanishing gradient problem by providing small-slope outputs for negative inputs, ensuring that potentially valuable information is retained. On the other hand, the decoder uses two types of modules of the form ConvTranspose-BatchNorm-Dropout-ReLU and ConvTranspose-BatchNorm-ReLU. The Dropout layer randomly deactivates half of the input units, introducing stochasticity to enhance network generalization. Additionally, we adopt the U-Net architecture as the backbone of  $G$  to learn semantic context information. In a mathematical formulation,  $G$  can be represented as  $\tilde{\mathbf{I}}^U = Dec[Enc(\hat{\mathbf{I}}^U)]$ , where  $Enc$  denotes the encoder,  $Dec$  denotes the decoder, and  $\tilde{\mathbf{I}}^U$  denotes the restored image.

Discriminator  $D$  also uses modules of the form Convolution-BatchNorm-LeakyReLU. Nevertheless, it takes two pairs of images concatenated together as input.  $D$  is trained to distinguish between fake image ( $\tilde{\mathbf{I}}^U$  generated from  $G$ ) and real image (the input undamaged road image  $\mathbf{I}^U$ ) conditioned on the corrupted image  $\hat{\mathbf{I}}^U$ .

#### D. Road Crack Detection

In the testing phase, given a damaged road image  $\mathbf{I}^D$ , the detection results  $\mathbf{S}$  can be obtained using the following expression:

$$\mathbf{S} = O[B((\tilde{\mathbf{I}}^D - \mathbf{I}^D) \odot (\tilde{\mathbf{I}}^D - \mathbf{I}^D))], \quad (1)$$

where  $\tilde{\mathbf{I}}^D$  denotes the restored image,  $B$  denotes the bilateral filtering [48] operation used to reduce small incorrectly detected regions for improved road crack detection performance, and  $O$  denotes the Otsu's thresholding [49] operation to binarize error maps for pixel-wise crack detection.

#### E. Loss Functions

The total loss function is as follows:

$$\mathcal{L}_{total} = \lambda_{res}\mathcal{L}_{res} + \lambda_{adv}\mathcal{L}_{adv}, \quad (2)$$

where  $\lambda_{res}$  and  $\lambda_{adv}$  are hyper-parameters used to balance the restoration loss  $\mathcal{L}_{res}$  and the adversarial loss  $\mathcal{L}_{adv}$ .  $G$  is updated by minimizing  $\mathcal{L}_{total}$ , while  $D$  is updated by maximizing  $\mathcal{L}_{adv}$ .

1) *Restoration Loss*: We use the mean average error (MAE) loss to measure the difference between  $\mathbf{I}^U$  and  $\tilde{\mathbf{I}}^U$ :

$$\mathcal{L}_{MAE} = \|\tilde{\mathbf{I}}^U - \mathbf{I}^U\|_1. \quad (3)$$

However, the MAE loss calculates the pixel intensity differences independently, ignoring the correlation between neighboring pixels. Therefore, we also use a structured similarity index measure (SSIM) loss [50] and a multi-scale gradient

magnitude similarity (MSGMS) loss [47] to measure the structural difference between them:

$$\mathcal{L}_{SSIM} = \frac{1}{H \times W} \sum_{i=1}^H \sum_{j=1}^W [1 - SSIM(\mathbf{I}^U, \tilde{\mathbf{I}}^U)_{(i,j)}], \quad (4)$$

$$\mathcal{L}_{MSGMS} = \frac{1}{4} \sum_{l=1}^4 \frac{1}{N_l} \sum_{i=1}^{H_l} \sum_{j=1}^{W_l} [1 - GMS(\mathbf{I}^U, \tilde{\mathbf{I}}^U)_{(i,j)}], \quad (5)$$

where  $SSIM$  refers to the SSIM value [50] between two patches of  $\mathbf{I}^U$  and  $\tilde{\mathbf{I}}^U$  centered at pixel  $(i, j)$ . The MSGMS loss is calculated over an image pyramid of four different scales, including the original image, and images that are  $\frac{1}{2}$ ,  $\frac{1}{4}$ , and  $\frac{1}{8}$  of the original size.  $H_l$  and  $W_l$  represent the height and width of the image at scale  $l$ , respectively, and  $N_l$  denotes the number of pixels at scale  $l$ , respectively.  $GMS$  refers to the value of GMS map [51] of  $\mathbf{I}^U$  and  $\tilde{\mathbf{I}}^U$  at pixel  $(i, j)$ . Additionally, we employ a style loss [52] as follows:

$$\mathcal{L}_{style} = \mathbb{E}_i[|G_i^\phi(\tilde{\mathbf{I}}^U) - G_i^\phi(\mathbf{I}^U)|] \quad (6)$$

to measure the feature difference between  $\mathbf{I}^U$  and  $\tilde{\mathbf{I}}^U$ , where  $G_i^\phi$  represents a  $C_i \times C_i$  gram matrix constructed from  $\phi_i$ , which denotes the activation map of the  $i$ -th layer of the pre-trained network. Therefore, the total restoration loss is formulated as follows:

$$\mathcal{L}_{res} = \lambda_{mae}\mathcal{L}_{MAE} + \lambda_{ssim}\mathcal{L}_{SSIM} + \lambda_{gms}\mathcal{L}_{MSGMS} + \lambda_{style}\mathcal{L}_{style}, \quad (7)$$

where  $\lambda_{mae}$ ,  $\lambda_{ssim}$ ,  $\lambda_{gms}$  and  $\lambda_{style}$  are hyper-parameters used to balance these losses.

2) *Adversarial loss*: The adversarial loss is formulated as follows:

$$\mathcal{L}_{adv}(G, D) = \mathbb{E}_{\hat{\mathbf{I}}^U, \mathbf{I}^U}[\log D(\hat{\mathbf{I}}^U, \mathbf{I}^U)] + \mathbb{E}_{\hat{\mathbf{I}}^U, z}[\log(1 - D(\hat{\mathbf{I}}^U, G(\hat{\mathbf{I}}^U, z))], \quad (8)$$

where  $\hat{\mathbf{I}}^U = G(\hat{\mathbf{I}}^U, z)$  and  $z$  denotes random noise introduced by the dropout layers.

## IV. EXPERIMENTAL RESULTS

### A. Datasets

The **Crack500** [53] dataset contains 500 images (resolution:  $2,000 \times 1,500$  pixels) of pavement cracks. These images have been annotated at the pixel level. Each image is cropped into 16 non-overlapped image regions, with only those regions containing more than 1,000 pixels of cracks being retained. This process yields a total of 1,896 training images, 348 validation images, and 1,124 test images. In our experiments, we use the original dataset to train supervised methods. Additionally, we crop 1,896 undamaged road images from the original images to train unsupervised methods. It is important to note that the Crack500 dataset poses significant challenges for practical crack detection, as it includes shadows, occlusions, and varying lighting conditions.

The **DeepCrack** [3] dataset contains 537 concrete surface images (resolution:  $544 \times 384$  pixels) with multi-scale and

TABLE I: Ablation study results for pixel-wise crack detection performance using five loss functions with the proposed UP-CrackNet on the Crack500 dataset [53]. The symbol ✓ indicates the selected loss function.

$\mathcal{L}_{MAE}$	$\mathcal{L}_{SSIM}$	$\mathcal{L}_{MSGMS}$	$\mathcal{L}_{style}$	$\mathcal{L}_{adv}$	Precision (%)↑	Recall (%)↑	Accuracy (%)↑	F1-Score (%)↑	IoU (%)↑
✓					60.026	29.387	89.704	39.457	24.577
✓	✓				71.705	40.326	92.488	51.621	34.790
✓		✓			55.188	53.561	94.821	54.363	37.327
✓			✓		57.074	35.620	91.835	43.864	28.093
✓				✓	60.876	57.502	95.299	59.141	41.986
✓	✓	✓			75.341	48.014	94.063	58.651	41.494
✓	✓	✓	✓		<b>76.651</b>	48.533	94.152	59.434	42.282
✓	✓	✓		✓	59.239	<b>61.021</b>	<b>95.607</b>	60.116	42.976
✓	✓	✓	✓	✓	65.377	58.609	95.484	<b>61.808</b>	<b>44.726</b>

TABLE II: Ablation study results using different modes of masks on the Crack500 dataset [53].

Mode	Accuracy (%)↑	F1-Score (%)↑	IoU (%)↑
$M_{Jumbled}$	94.057	48.728	32.213
$M_{Striped}$	95.379	58.932	41.775
$M_{Mul-S}$	<b>95.484</b>	<b>61.808</b>	<b>44.726</b>

multi-scene cracks. These images have also been annotated at the pixel level. The dataset is divided into two subsets, with 300 images used for training and the remaining 237 images used for testing. Similarly, we use the original dataset to train supervised methods, and from the same dataset, we extract 300 undamaged road images to train unsupervised methods.

The CFD [54] dataset contains 118 concrete surface images (resolution:  $480 \times 320$  pixels), manually annotated at the pixel level. These images exhibit diverse illumination conditions, shadows, and stains, making the detection of cracks challenging. We extract 200 image patches (resolution:  $256 \times 256$  pixels) to evaluate the generalizability of both supervised and unsupervised methods.

### B. Implementation Details & Evaluation Metrics

Our experiments are conducted on a single NVIDIA RTX3090. The models are trained for 200 epochs, with early stopping if there is no performance improvement on the validation set for 20 consecutive epochs. All images are resized to  $256 \times 256$  pixels, and data augmentation techniques including scaling, cropping, and flipping are applied. Stochastic gradient descent (SGD) is used to optimize networks, with a momentum value of 0.9 and weight decay set to  $10^{-4}$ . The initial learning rate is set to 0.01 and is dynamically adjusted using the poly strategy. The training settings of UP-CrackNet follow the well-known Pix2Pix [55], where an Adam optimizer [56] with  $\beta_1 = 0.5$  and  $\beta_2 = 0.999$  is used to optimize the networks. The initial learning rates for the generator  $G$  and discriminator  $D$  are set to 0.0001 and 0.0004, respectively. During training, the learning rates decay exponentially. The hyper-parameters in the loss functions are set to  $\lambda_{mae} = \lambda_{ssim} = \lambda_{gms} = 1$ ,  $\lambda_{style} = 10$ ,  $\lambda_{res} = 100$ , and  $\lambda_{adv} = 1$ . In our implementation,  $H$  and  $W$  are set to 256, and  $k$  is set to  $\{128, 64, 32\}$ . For evaluation, we use precision, recall, accuracy, intersection

over union (IoU), and F1-score to quantitatively compare UP-CrackNet with other methods.

### C. Ablation Study

To analyze the effectiveness of the five employed losses, we conduct an ablation study on the Crack500 dataset. The quantitative results presented in Table I suggest that each loss contributes to improved road crack detection results, and our method, incorporating all these losses, achieves the best performance. Notably, the adversarial loss  $\mathcal{L}_{adv}$  provides the most significant improvement among these losses.

To validate the effectiveness of the designed multi-scale square masks, we conduct another ablation study on the same dataset using different modes of masks. The comparison results are given in Table II, where  $M_{Mul-S}$  denotes our designed multi-scale square masks,  $M_{Striped}$  denotes striped masks used in SCADN, and  $M_{Jumbled}$  denotes jumbled small square masks used in RIAD. These results indicate that our method achieves improvements of 2.876% and 13.080% in F1-Score, as well as improvements of 2.951% and 12.513% in IoU compared to using the other two types of masks.

### D. Comparison with Other SoTA Methods

We compare our proposed UP-CrackNet with 11 general supervised semantic segmentation methods, two supervised crack detection-specific methods, and two general image restoration-based unsupervised anomaly detection methods on the Crack500 and Deepcrack datasets. The quantitative and qualitative comparison results are shown in Table III, Table IV, Fig. 2 and Fig. 3, respectively. It can be observed that UP-CrackNet achieves satisfactory detection performance compared with supervised methods and performs much better than other general image restoration-based unsupervised methods.

Specifically, on the Crack500 dataset, our proposed UP-CrackNet has 1.185% – 6.355% and 8.194% – 9.877% reduction in IoU than the general and crack detection-specific supervised methods, respectively. On the Deepcrack dataset [3], UP-CrackNet achieves better performance than all general supervised methods and has 4.665% – 6.814% reduction in IoU than specific supervised methods. Considering supervised methods require a large amount of human-annotated pixel-level labels, our proposed UP-CrackNet with satisfactory detection performance has strong application prospects.

TABLE III: Quantitative experimental results on the Crack500 dataset [53].

Training Strategy	Methods	Precision (%)↑	Recall (%)↑	Accuracy (%)↑	F1-Score (%)↑	IoU (%)↑
General Supervised	DeepLabv3+ [38]	58.442	68.165	96.152	62.930	45.911
	ENet [57]	57.544	65.505	95.933	61.267	44.162
	PSPNet [58]	61.665	69.271	96.329	65.247	48.420
	UperNet [59]	59.134	<b>72.275</b>	96.448	65.048	48.200
	SegResNet [35]	58.777	64.229	95.866	61.382	44.282
	UNet [60]	72.465	56.611	95.357	63.565	46.589
	BiSeNetv2 [61]	69.332	64.176	96.122	66.655	49.986
	DDRNet [62]	55.727	68.637	96.102	61.512	44.417
	Lawin [63]	69.413	65.919	96.284	67.621	51.081
Specific Supervised	Deepcrack19 [3]	<b>86.733</b>	57.581	95.687	69.213	52.920
	Deepcrack18 [1]	70.356	70.919	<b>96.731</b>	<b>70.636</b>	<b>54.603</b>
Unsupervised	SCADN [46]	46.723	14.064	81.064	21.620	12.120
	RIAD [47]	65.420	11.665	70.374	19.799	10.987
Proposed	UP-CrackNet	65.377	58.609	95.484	61.808	44.726

TABLE IV: Quantitative experimental results on the Deepcrack dataset [3].

Training Strategy	Methods	Precision (%)↑	Recall (%)↑	Accuracy (%)↑	F1-Score (%)↑	IoU (%)↑
General Supervised	DeepLabv3+ [38]	68.078	79.690	97.842	73.428	58.013
	ENet [57]	66.618	82.529	97.921	73.725	58.385
	PSPNet [58]	44.872	85.280	97.247	58.803	41.646
	UperNet [59]	67.001	82.344	97.926	73.884	58.585
	SegResNet [35]	37.615	82.334	96.915	51.639	34.806
	UNet [60]	46.530	88.690	97.399	61.038	43.924
	BiSeNetv2 [61]	64.428	79.970	97.736	71.363	55.476
	DDRNet [62]	45.270	62.123	96.395	52.374	35.478
	Lawin [63]	62.249	84.282	97.839	71.609	55.774
Specific Supervised	Deepcrack19 [3]	88.785	68.923	97.756	77.603	63.403
	Deepcrack18 [1]	71.720	88.403	<b>98.350</b>	<b>79.192</b>	<b>65.552</b>
Unsupervised	SCADN [46]	66.879	34.128	92.897	45.194	29.194
	RIAD [47]	<b>90.079</b>	20.742	84.494	33.720	20.279
Proposed	UP-CrackNet	63.412	<b>88.852</b>	98.049	74.006	58.738

TABLE V: Quantitative experimental results on the CFD dataset [54] (all trained on the Crack500 dataset [53]).

Training Strategy	Methods	Precision (%)↑	Recall (%)↑	Accuracy (%)↑	F1-Score (%)↑	IoU (%)↑
General Supervised	DeepLabv3+ [38]	6.736	54.663	98.277	11.994	6.380
	ENet [57]	0.123	0.206	98.261	0.156	0.078
	PSPNet [58]	11.364	52.256	98.274	18.668	10.295
	UperNet [59]	7.174	<b>55.643</b>	<b>98.282</b>	12.709	6.786
	SegResNet [35]	0.088	0.739	98.052	0.157	0.079
	UNet [60]	15.674	48.025	98.235	23.634	13.401
	BiSeNetv2 [61]	18.85	21.058	97.353	19.892	11.045
	DDRNet [62]	0.084	31.993	98.255	0.167	0.083
	Lawin [63]	38.508	37.250	97.797	37.869	23.357
Specific Supervised	Deepcrack19 [3]	<b>95.215</b>	29.446	95.940	44.981	29.017
	Deepcrack18 [1]	77.500	43.759	97.872	<b>55.935</b>	<b>38.826</b>
Unsupervised	SCADN [46]	43.424	15.343	94.837	22.674	12.787
	RIAD [47]	93.619	11.553	87.395	20.568	11.463
Proposed	UP-CrackNet	63.161	41.253	97.790	49.909	33.252

Compared with two unsupervised methods, our proposed UP-CrackNet achieves an increase of 32.606% – 33.739% and 29.544%–38.459% IoU improvement on the Crack500 dataset [53] and Deepcrack dataset [3], respectively. These results demonstrate that our designed model and losses are more effective for unsupervised pixel-wise crack detection.

### E. Generalizability Evaluation

To further evaluate the generalizability of the compared methods, we assess the performance of networks trained on the

Crack500 dataset and the Deepcrack dataset on other datasets. The quantitative comparison results are shown in Tables V, VI, VII, and VIII, respectively. These results indicate that our proposed UP-CrackNet has superior generalizability than other supervised and unsupervised methods.

When UP-CrackNet is trained on the Crack500 dataset and tested on the Deepcrack dataset, it demonstrates IoU improvements ranging from 3.067% to 45.892%. Conversely, when the training and test sets are switched, UP-CrackNet still demonstrates substantial IoU improvements, ranging from



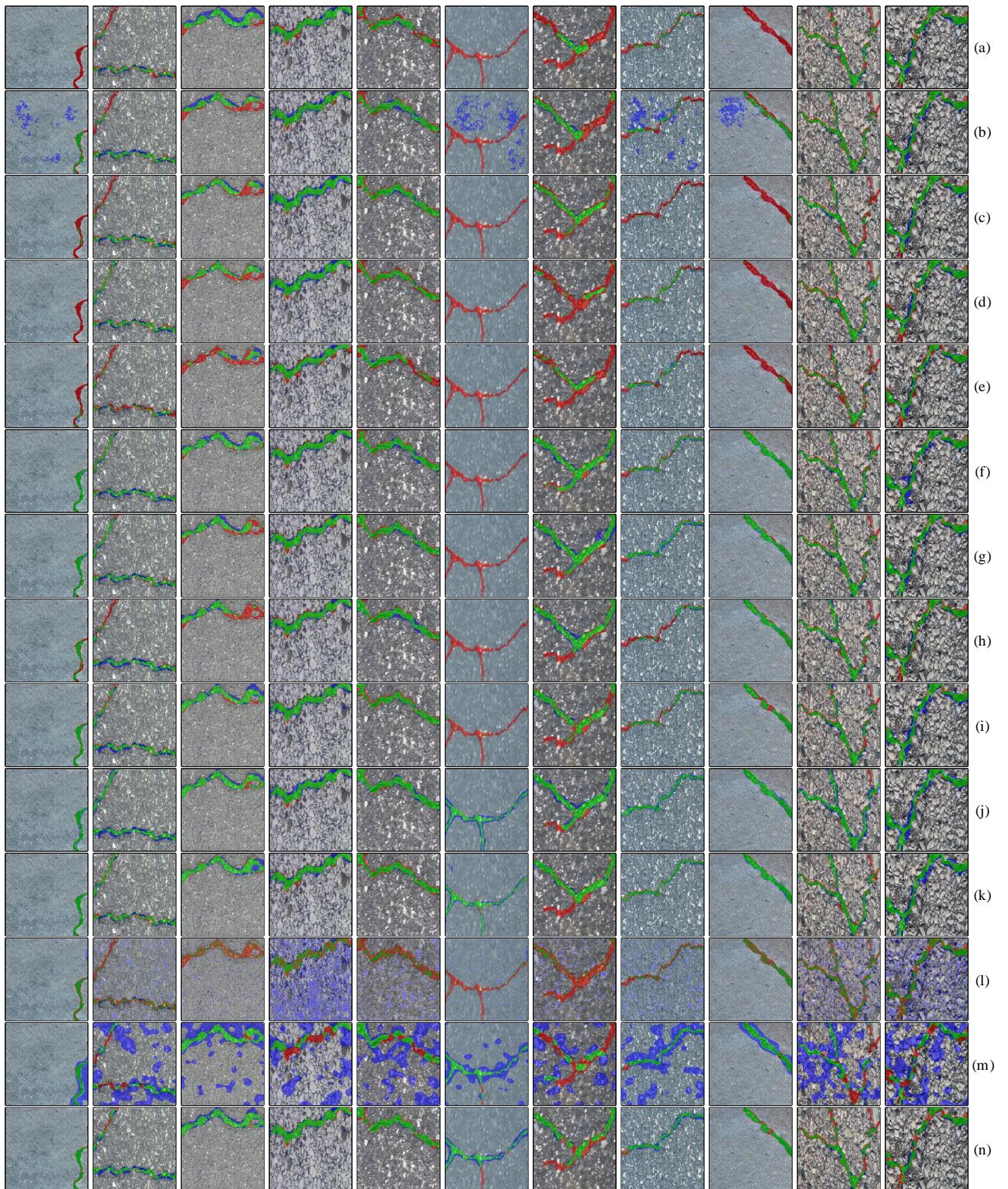


Fig. 2: Examples of experimental results on the Crack500 dataset: (a) DeepLabv3+ [38]; (b) ENet [57]; (c) PSPNet [58]; (d) UperNet [59]; (e) SegResNet [35]; (f) UNet [60]; (g) BiSeNetv2 [61]; (h) DDRNet [62]; (i) Lawin [63]; (j) Deepcrack19 [3]; (k) Deepcrack18 [1]; (l) SCADN [46]; (m) RIAD [47]; (n) UP-CrackNet. The true-positive, false-positive, and false-negative pixels are shown in green, blue, and red, respectively.



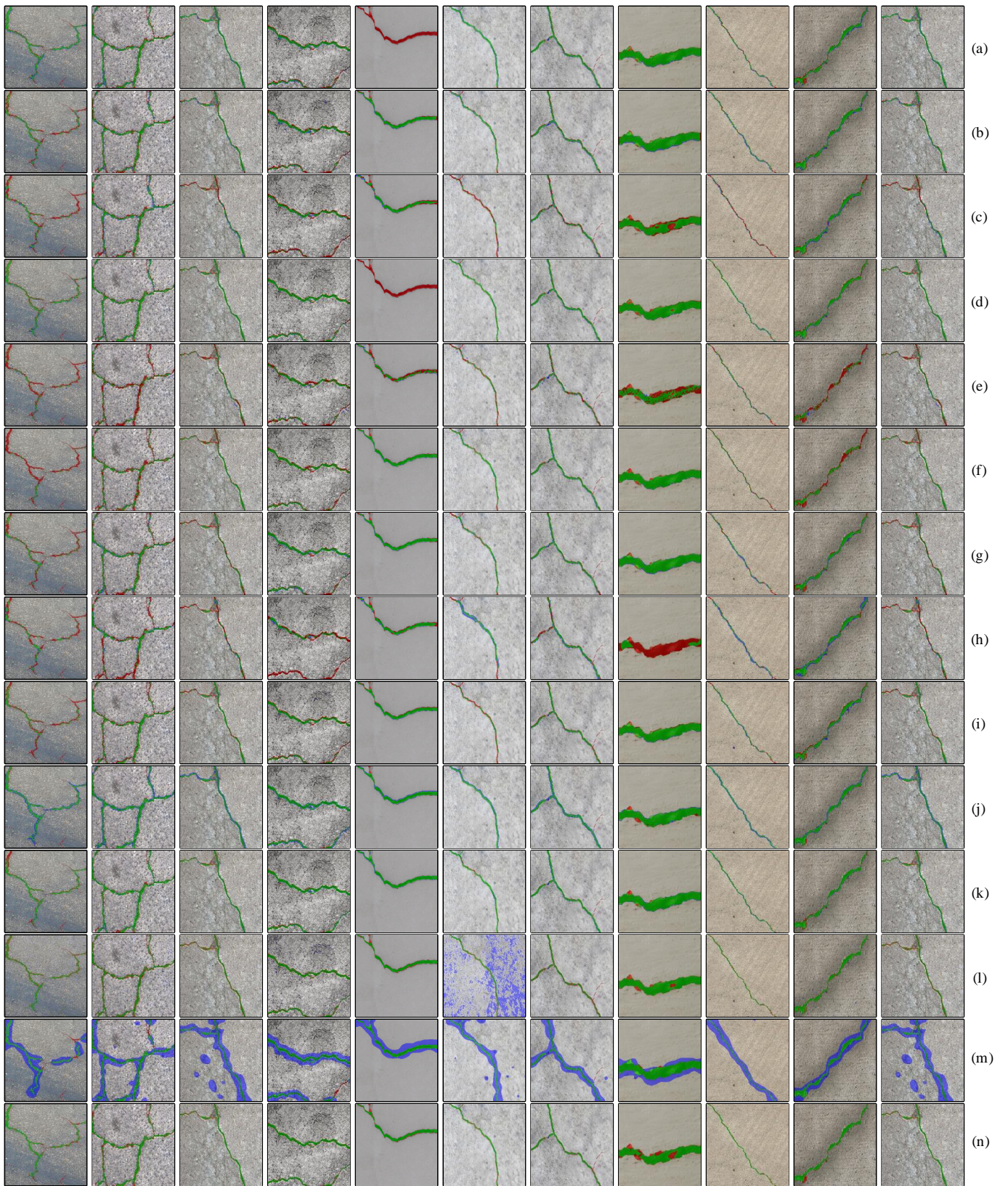


Fig. 3: Examples of experimental results on the Deepcrack dataset [3]:(a) DeepLabv3+ [38]; (b) ENet [57]; (c) PSPNet [58]; (d) UperNet [59]; (e) SegResNet [35]; (f) UNet [60]; (g) BiSeNetv2 [61]; (h) DDRNet [62]; (i) Lawin [63]; (j) Deepcrack19 [3]; (k) Deepcrack18 [1]; (l) SCADN [46]; (m) RIAD [47]; (n) UP-CrackNet. The true-positive, false-positive, and false-negative pixels are shown in green, blue, and red, respectively.



TABLE VI: Quantitative experimental results on the Deepcrack dataset [3] (all trained on the Crack500 dataset [53]).

Training Strategy	Methods	Precision (%)↑	Recall (%)↑	Accuracy (%)↑	F1-Score (%)↑	IoU (%)↑
General Supervised	DeepLabv3+ [38]	41.074	32.452	93.716	36.258	22.143
	ENet [57]	63.108	37.842	93.884	47.313	30.987
	PSPNet [58]	31.923	73.212	96.529	44.460	28.584
	UperNet [59]	29.161	66.696	96.284	40.579	25.454
	SegResNet [35]	50.286	36.141	93.971	42.056	26.627
	UNet [60]	79.396	22.930	87.492	35.583	21.642
	BiSeNetv2 [61]	76.207	20.107	85.795	31.819	18.920
	DDRNet [62]	38.233	64.599	96.402	48.036	31.610
	Lawin [63]	54.994	63.056	96.641	58.749	41.592
Specific Supervised	Deepcrack19 [3]	<b>95.828</b>	48.461	95.384	64.370	47.460
	Deepcrack18 [1]	90.349	61.837	97.154	73.422	58.006
Unsupervised	SCADN [46]	59.006	16.970	85.660	26.360	15.181
	RIAD [47]	86.545	16.620	80.529	27.884	16.201
Proposed	UP-CrackNet	72.464	<b>79.531</b>	<b>97.990</b>	<b>75.833</b>	<b>61.073</b>

TABLE VII: Quantitative experimental results on the CFD dataset [54] (all trained on the Deepcrack dataset [3]).

Training Strategy	Methods	Precision (%)↑	Recall (%)↑	Accuracy (%)↑	F1-Score (%)↑	IoU (%)↑
General Supervised	DeepLabv3+ [38]	37.292	48.669	98.221	42.228	26.765
	ENet [57]	17.826	50.529	98.263	26.354	15.177
	PSPNet [58]	22.725	42.553	98.118	29.627	17.390
	UperNet [59]	31.493	51.817	98.295	39.176	24.360
	SegResNet [35]	16.102	48.689	98.242	24.200	13.766
	UNet [60]	25.609	53.281	98.312	34.592	20.913
	BiSeNetv2 [61]	15.706	49.193	98.248	23.810	13.514
	DDRNet [62]	9.153	46.625	98.234	15.301	8.285
	Lawin [63]	14.903	<b>55.158</b>	98.305	23.466	13.292
Specific Supervised	Deepcrack19 [3]	77.205	38.407	97.444	<b>51.296</b>	<b>34.495</b>
	Deepcrack18 [1]	35.837	54.237	<b>98.354</b>	43.158	27.517
Unsupervised	SCADN [46]	64.689	8.626	87.439	15.222	8.238
	RIAD [47]	<b>92.259</b>	10.824	86.614	19.374	10.726
Proposed	UP-CrackNet	52.388	42.267	97.923	46.787	30.537

TABLE VIII: Quantitative experimental results on the Crack500 dataset [53] (all trained on the Deepcrack dataset [3]).

Training Strategy	Methods	Precision (%)↑	Recall (%)↑	Accuracy (%)↑	F1-Score (%)↑	IoU (%)↑
General Supervised	DeepLabv3+ [38]	33.991	44.695	93.959	38.615	23.927
	ENet [57]	15.590	54.308	94.548	24.226	13.782
	PSPNet [58]	8.285	<b>85.049</b>	94.792	15.099	8.166
	UperNet [59]	46.681	42.171	93.441	44.311	28.462
	SegResNet [35]	8.720	64.049	94.624	15.349	8.313
	UNet [60]	5.656	47.105	94.371	10.099	5.318
	BiSeNetv2 [61]	20.450	40.461	93.871	27.169	15.720
	DDRNet [62]	40.761	16.881	85.470	23.875	13.555
	Lawin [63]	20.272	76.551	95.196	32.055	19.087
Specific Supervised	Deepcrack19 [3]	61.160	51.056	94.552	55.653	38.555
	Deepcrack18 [1]	21.196	77.557	<b>95.252</b>	33.294	19.971
Unsupervised	SCADN [46]	49.131	14.896	81.466	22.861	12.906
	RIAD [47]	<b>67.502</b>	12.413	71.558	20.969	11.713
Proposed	UP-CrackNet	62.796	52.200	94.706	<b>57.010</b>	<b>39.870</b>

1.315% to 34.552%. We attribute these improvements in generalizability to the efficacy of unsupervised image restoration, which allows the model to restore the corrupted regions by analyzing the context provided by surrounding patches. This capacity to capture meaningful semantic information from neighboring contexts significantly enhances UP-CrackNet’s performance across different datasets and test scenarios. It is worth noting that although UP-CrackNet performs slightly worse than Deepcrack19 when evaluated on the CFD dataset,

we believe this discrepancy is primarily attributed to the dataset itself. The CFD dataset contains small and thin road cracks, making it challenging for image restoration-based algorithms to preserve the clear boundaries of these cracks.

## V. DISCUSSION

As discussed above, it is imperative to divide a given road crack dataset into two sets of road image patches: one containing road cracks and the other free of any cracks. This

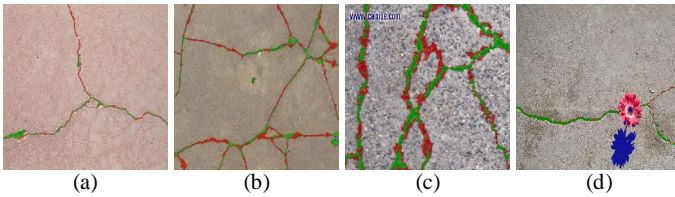


Fig. 4: Failure cases of UP-CrackNet on the Deepcrack dataset [3]. The true-positive, false-positive, and false-negative pixels are shown in green, blue, and red, respectively.

separation is a fundamental step in training UP-CrackNet, allowing the model to effectively restore undamaged road regions. Fortunately, road crack detection is a relatively easy image classification task, as has been quantitatively demonstrated in [20]. Therefore, after extracting image patches from the original images within road crack datasets, pre-trained crack classification networks can be employed to accurately identify undamaged road image patches, which are subsequently fed into UP-CrackNet.

We also present some instances where UP-CrackNet encounters challenges on the Deepcrack dataset [3] in Fig. 4. (a) and (b) illustrate situations where UP-CrackNet sometimes does not perform as expected when detecting thin cracks. This can occur because our method may occasionally categorize these small and thin cracks as undamaged regions, resulting in their restoration to their original appearance and, consequently, missed detection. (c) and (d) illustrate cases where UP-CrackNet erroneously identifies image watermark digits and shadows of flowers as damaged areas. This happens because these patterns either do not appear or occur very rarely in the training set. Consequently, UP-CrackNet fails to restore them to their original appearance, leading to false detections. To address these challenges, future work can focus on developing more advanced training mechanisms and network architectures to enhance the detection of thin cracks. Additionally, improving the robustness and intelligence of UP-CrackNet to distinguish between road cracks and other anomalies is an area that warrants further research and development.

## VI. CONCLUSION

This article introduced UP-CrackNet, a novel network architecture and training paradigm designed to overcome the limitations of previous supervised pixel-wise road crack detection algorithms. The training of UP-CrackNet was exclusively performed using undamaged road image patches, where an adversarial image restoration technique was applied to learn corrupted regions in an unsupervised manner. The testing process involves a series of conventional image processing algorithms, including bilateral filtering and Otsu's thresholding. Extensive experiments conducted on three datasets demonstrate the effectiveness of our UP-CrackNet in detecting road cracks and its superior generalizability across different datasets and scenarios. In the future, we intend to investigate alternative training strategies and network architectures to further improve UP-CrackNet's performance in detecting thin cracks. Additionally, conducting real-world experiments

involving automatic road inspection robots or vehicles is also part of our future research endeavors.

## REFERENCES

- [1] Q. Zou *et al.*, "Deepcrack: Learning hierarchical convolutional features for crack detection," *IEEE Transactions on Image Processing*, vol. 28, no. 3, pp. 1498–1512, 2018.
- [2] J. S. Miller *et al.*, "Distress identification manual for the long-term pavement performance program," United States. Federal Highway Administration. Office of Infrastructure Research and Development, Tech. Rep., 2003.
- [3] Y. Liu *et al.*, "Deepcrack: A deep hierarchical feature learning architecture for crack segmentation," *Neurocomputing*, vol. 338, pp. 139–153, 2019.
- [4] R. Fan *et al.*, "Road surface 3D reconstruction based on dense subpixel disparity map estimation," *IEEE Transactions on Image Processing*, vol. 27, no. 6, pp. 3025–3035, 2018.
- [5] N. Ma *et al.*, "Computer vision for road imaging and pothole detection: a state-of-the-art review of systems and algorithms," *Transportation Safety and Environment*, vol. 4, no. 4, p. tdac026, 2022.
- [6] J. Li *et al.*, "Roadformer: Duplex transformer for rgb-normal semantic road scene parsing," *IEEE Transactions on Intelligent Vehicles*, 2024.
- [7] R. Fan and M. Liu, "Road damage detection based on unsupervised disparity map segmentation," *IEEE Transactions on Intelligent Transportation Systems*, vol. 21, no. 11, pp. 4906–4911, 2020.
- [8] R. Fan *et al.*, "Pothole detection based on disparity transformation and road surface modeling," *IEEE Transactions on Image Processing*, vol. 29, pp. 897–908, 2019.
- [9] R. Fan *et al.*, "Graph attention layer evolves semantic segmentation for road pothole detection: A benchmark and algorithms," *IEEE Transactions on Image Processing*, vol. 30, pp. 8144–8154, 2021.
- [10] R. Fan *et al.*, "Rethinking road surface 3-D reconstruction and pothole detection: From perspective transformation to disparity map segmentation," *IEEE Transactions on Cybernetics*, vol. 52, no. 7, pp. 5799–5808, 2022.
- [11] G. Zhao *et al.*, "Anisotropic clustering on surfaces for crack extraction," *Machine Vision and Applications*, vol. 26, pp. 675–688, 2015.
- [12] A. Ayenu-Prah and N. Attoh-Okine, "Evaluating pavement cracks with bidimensional empirical mode decomposition," *EURASIP Journal on Advances in Signal Processing*, vol. 2008, pp. 1–7, 2008.
- [13] T. Yamaguchi *et al.*, "Image-based crack detection for real concrete surfaces," *IEEE Transactions on Electrical and Electronic Engineering*, vol. 3, no. 1, pp. 128–135, 2008.
- [14] Y. Hu and C. Zhao, "A novel LBP based methods for pavement crack detection," *Journal of Pattern Recognition Research*, vol. 5, no. 1, pp. 140–147, 2010.
- [15] J. Zhou *et al.*, "Wavelet-based pavement distress detection and evaluation," *Optical Engineering*, vol. 45, no. 2, pp. 027 007–027 007, 2006.
- [16] R. Amhaz *et al.*, "Automatic crack detection on two-dimensional pavement images: An algorithm based on minimal path selection," *IEEE Transactions on Intelligent Transportation Systems*, vol. 17, no. 10, pp. 2718–2729, 2016.
- [17] R. Fan *et al.*, "Road crack detection using deep convolutional neural network and adaptive thresholding," in *2019 IEEE Intelligent Vehicles Symposium (IV)*. IEEE, 2019, pp. 474–479.
- [18] S. Guo *et al.*, "UDTIRI: An online open-source intelligent road inspection benchmark suite," *IEEE Transactions on Intelligent Transportation System*, 2024.
- [19] A. Krizhevsky *et al.*, "Imagenet classification with deep convolutional neural networks," *Communications of the ACM*, vol. 60, no. 6, pp. 84–90, 2017.
- [20] J. Fan *et al.*, "Deep convolutional neural networks for road crack detection: Qualitative and quantitative comparisons," in *2021 IEEE International Conference on Imaging Systems and Techniques (IST)*. IEEE, 2021, pp. 1–6.
- [21] Y.-J. Cha *et al.*, "Autonomous structural visual inspection using region-based deep learning for detecting multiple damage types," *Computer-Aided Civil and Infrastructure Engineering*, vol. 33, no. 9, pp. 731–747, 2018.
- [22] Y. Du *et al.*, "Pavement distress detection and classification based on yolo network," *International Journal of Pavement Engineering*, vol. 22, no. 13, pp. 1659–1672, 2021.
- [23] C. V. Dung *et al.*, "Autonomous concrete crack detection using deep fully convolutional neural network," *Automation in Construction*, vol. 99, pp. 52–58, 2019.

- [24] J. Huyan *et al.*, “CrackU-Net: A novel deep convolutional neural network for pixelwise pavement crack detection,” *Structural Control and Health Monitoring*, vol. 27, no. 8, p. e2551, 2020.
- [25] Z. Qu *et al.*, “A crack detection algorithm for concrete pavement based on attention mechanism and multi-features fusion,” *IEEE Transactions on Intelligent Transportation Systems*, vol. 23, no. 8, pp. 11 710–11 719, 2021.
- [26] T. Chen *et al.*, “Pavement crack detection and recognition using the architecture of segnet,” *Journal of Industrial Information Integration*, vol. 18, p. 100144, 2020.
- [27] J. Liu *et al.*, “Automated pavement crack detection and segmentation based on two-step convolutional neural network,” *Computer-Aided Civil and Infrastructure Engineering*, vol. 35, no. 11, pp. 1291–1305, 2020.
- [28] A. A. Zhang *et al.*, “Intelligent pixel-level detection of multiple distresses and surface design features on asphalt pavements,” *Computer-Aided Civil and Infrastructure Engineering*, vol. 37, no. 13, pp. 1654–1673, 2022.
- [29] G. Zhu *et al.*, “A lightweight encoder–decoder network for automatic pavement crack detection,” *Computer-Aided Civil and Infrastructure Engineering*, 2023.
- [30] P. Subirats *et al.*, “Automation of pavement surface crack detection using the continuous wavelet transform,” in *2006 International Conference on Image Processing (ICIP)*. IEEE, 2006, pp. 3037–3040.
- [31] R. Amhaz *et al.*, “A new minimal path selection algorithm for automatic crack detection on pavement images,” in *2014 IEEE International Conference on Image Processing (ICIP)*. IEEE, 2014, pp. 788–792.
- [32] H. Tsuchiya *et al.*, “A method of data augmentation for classifying road damage considering influence on classification accuracy,” *Procedia Computer Science*, vol. 159, pp. 1449–1458, 2019.
- [33] G. X. Hu *et al.*, “Pavement crack detection method based on deep learning models,” *Wireless Communications and Mobile Computing*, vol. 2021, pp. 1–13, 2021.
- [34] K. Simonyan and A. Zisserman, “Very deep convolutional networks for large-scale image recognition,” *arXiv preprint arXiv:1409.1556*, 2014.
- [35] V. Badrinarayanan *et al.*, “Segnet: A deep convolutional encoder-decoder architecture for image segmentation,” *IEEE Transactions on Pattern Analysis and Machine Intelligence*, vol. 39, no. 12, pp. 2481–2495, 2017.
- [36] G. Zhu *et al.*, “RHA-Net: An encoder-decoder network with residual blocks and hybrid attention mechanisms for pavement crack segmentation,” *arXiv preprint arXiv:2207.14166*, 2022.
- [37] X. Sun *et al.*, “DMA-Net: Deeplab with multi-scale attention for pavement crack segmentation,” *IEEE Transactions on Intelligent Transportation Systems*, vol. 23, no. 10, pp. 18 392–18 403, 2022.
- [38] L.-C. Chen *et al.*, “Encoder-decoder with atrous separable convolution for semantic image segmentation,” in *Proceedings of the European Conference on Computer Vision (ECCV)*, 2018, pp. 801–818.
- [39] H. Yang *et al.*, “Multiscale feature-clustering-based fully convolutional autoencoder for fast accurate visual inspection of texture surface defects,” *IEEE Transactions on Automation Science and Engineering*, vol. 16, no. 3, pp. 1450–1467, 2019.
- [40] Y. Shi *et al.*, “Unsupervised anomaly segmentation via deep feature reconstruction,” *Neurocomputing*, vol. 424, pp. 9–22, 2021.
- [41] D. Dehaene *et al.*, “Iterative energy-based projection on a normal data manifold for anomaly localization,” in *International Conference on Learning Representations*, 2019.
- [42] Q. Zhou *et al.*, “Semi-supervised fabric defect detection based on image reconstruction and density estimation,” *Textile Research Journal*, vol. 91, no. 9–10, pp. 962–972, 2021.
- [43] T. Schlegl *et al.*, “f-AnoGAN: Fast unsupervised anomaly detection with generative adversarial networks,” *Medical image analysis*, vol. 54, pp. 30–44, 2019.
- [44] M. Sabokrou *et al.*, “Adversarially learned one-class classifier for novelty detection,” in *Proceedings of the IEEE Conference on Computer Vision and Pattern Recognition (CVPR)*. IEEE, 2018, pp. 3379–3388.
- [45] F. Ye *et al.*, “Attribute restoration framework for anomaly detection,” *IEEE Transactions on Multimedia*, vol. 24, pp. 116–127, 2020.
- [46] X. Yan *et al.*, “Learning semantic context from normal samples for unsupervised anomaly detection,” in *Proceedings of the AAAI Conference on Artificial Intelligence (AAAI)*, vol. 35, no. 4, 2021, pp. 3110–3118.
- [47] V. Zavrtanik *et al.*, “Reconstruction by inpainting for visual anomaly detection,” *Pattern Recognition*, vol. 112, p. 107706, 2021.
- [48] C. Tomasi and R. Manduchi, “Bilateral filtering for gray and color images,” in *Proceedings of the IEEE International Conference on Computer Vision (ICCV)*. IEEE, 1998, pp. 839–846.
- [49] N. Otsu, “A threshold selection method from gray-level histograms,” *IEEE Transactions on Systems, Man, and Cybernetics*, vol. 9, no. 1, pp. 62–66, 1979.
- [50] Z. Wang *et al.*, “Image quality assessment: from error visibility to structural similarity,” *IEEE Transactions on Image Processing*, vol. 13, no. 4, pp. 600–612, 2004.
- [51] W. Xue *et al.*, “Gradient magnitude similarity deviation: A highly efficient perceptual image quality index,” *IEEE Transactions on Image Processing*, vol. 23, no. 2, pp. 684–695, 2013.
- [52] J. Johnson *et al.*, “Perceptual losses for real-time style transfer and super-resolution,” in *Proceedings of the European Conference on Computer Vision (ECCV)*, 2016, pp. 694–711.
- [53] F. Yang *et al.*, “Feature pyramid and hierarchical boosting network for pavement crack detection,” *IEEE Transactions on Intelligent Transportation Systems*, vol. 21, no. 4, pp. 1525–1535, 2019.
- [54] Y. Shi *et al.*, “Automatic road crack detection using random structured forests,” *IEEE Transactions on Intelligent Transportation Systems*, vol. 17, no. 12, pp. 3434–3445, 2016.
- [55] P. Isola *et al.*, “Image-to-image translation with conditional adversarial networks,” in *Proceedings of the IEEE Conference on Computer Vision and Pattern Recognition (CVPR)*. IEEE, 2017, pp. 1125–1134.
- [56] D. P. Kingma and J. Ba, “Adam: A method for stochastic optimization,” *arXiv preprint arXiv:1412.6980*, 2014.
- [57] A. Paszke *et al.*, “ENet: A deep neural network architecture for real-time semantic segmentation,” *arXiv preprint arXiv:1606.02147*, 2016.
- [58] H. Zhao *et al.*, “Pyramid scene parsing network,” in *Proceedings of the IEEE Conference on Computer Vision and Pattern Recognition (CVPR)*. IEEE, 2017, pp. 2881–2890.
- [59] T. Xiao *et al.*, “Unified perceptual parsing for scene understanding,” in *Proceedings of the European Conference on Computer Vision (ECCV)*, 2018, pp. 418–434.
- [60] O. Ronneberger *et al.*, “U-net: Convolutional networks for biomedical image segmentation,” in *International Conference on Medical Image Computing and Computer-Assisted Intervention (MICCAI)*. Springer, 2015, pp. 234–241.
- [61] C. Yu *et al.*, “Bisenet v2: Bilateral network with guided aggregation for real-time semantic segmentation,” *International Journal of Computer Vision*, vol. 129, pp. 3051–3068, 2021.
- [62] H. Pan *et al.*, “Deep dual-resolution networks for real-time and accurate semantic segmentation of traffic scenes,” *IEEE Transactions on Intelligent Transportation Systems*, vol. 24, no. 3, pp. 3448–3460, 2022.
- [63] H. Yan *et al.*, “Lawin transformer: Improving semantic segmentation transformer with multi-scale representations via large window attention,” *arXiv preprint arXiv:2201.01615*, 2022.

**Nachuan Ma** is currently pursuing his Ph.D. degree at Tongji University with a research focus on visual perception techniques for autonomous driving.

**Rui Fan** (Senior Member, IEEE) is currently a Full Professor with the College of Electronics & Information Engineering and the Shanghai Research Institute for Intelligent Autonomous Systems at Tongji University. His research interests include computer vision, deep learning, and robotics.

**Lihua Xie** (Fellow, IEEE) has been a Professor and Director at the Center for Advanced Robotics Technology Innovation in the School of Electrical and Electronic Engineering at Nanyang Technological University, Singapore. Dr. Xie’s research interests include robust control and estimation, networked control systems, multi-agent networks, and unmanned systems.